CODEN IEJMAT *Internet Electronic Journal of Molecular Design* **2008**, *7*, 97–113 ISSN 1538–6414
BioChem Press http://www.biochempress.com

Inter*net* Electronic Journal of Molecular Design

May 2008, Volume 7, Number 5, Pages 97–113

Editor: Ovidiu Ivanciuc

The Calcium Ion and Conserved Water Molecules in Neuraminidases: Roles and Implications for Substrate Binding

Gang Yang,[1,2] Zhiwei Yang,[1] Yuangang Zu,[1] Xiaomin Wu,[1] and Yujie Fu [1]

[1] Key Laboratory of Forest Plant Ecology, Ministry of Education, Northeast Forestry University, Harbin 150040, P. R. China
[2] Dalian Institute of Chemical Physics, Chinese Academy of Sciences, Dalian 116023, P. R. China

Received: March 24, 2008; Revised: May 29, 2008; Accepted: May 30, 2008; Published: May 31, 2008

Citation of the article:
G. Yang, Z. Yang, Y. Zu, X. Wu, and Y. Fu, The Calcium Ion and Conserved Water Molecules in Neuraminidases: Roles and Implications for Substrate Binding, *Internet Electron. J. Mol. Des.* **2008**, *7*, 97–113, http://www.biochempress.com.

Inter*net* Electronic Journal of Molecular Design

BioChem Press
http://www.biochempress.com

The Calcium Ion and Conserved Water Molecules in Neuraminidases: Roles and Implications for Substrate Binding

Gang Yang,[1,2] Zhiwei Yang,[1] Yuangang Zu,[1,*] Xiaomin Wu,[1] and Yujie Fu [1]

[1] Key Laboratory of Forest Plant Ecology, Ministry of Education, Northeast Forestry University, Harbin 150040, P. R. China

[2] Dalian Institute of Chemical Physics, Chinese Academy of Sciences, Dalian 116023, P. R. China

Received: March 24, 2008; Revised: May 29, 2008; Accepted: May 30, 2008; Published: May 31, 2008

Internet Electron. J. Mol. Des. **2008**, *7* (5), 97–113

Abstract

Motivation. Neuraminidases are essential to the replication of influenza virus by catalyzing the cleavage of the α–ketosidic connection between the sugar residue and the sialic acid. Our aim in this paper was to study the roles of the calcium ion and conserved water molecules played during the substrate bindings towards the N9 subtype neuraminidase. In addition, the interaction modes between substrates and receptors were predicted based on structural and property analyses, which were confirmed by docking results.

Method. Molecular mechanics and molecular docking simulations as well as density functional calculations were performed using InsightII 2005 and Gaussian 98 software packages.

Results. With the inclusion of the calcium ion, the neuraminidase active site is close in both size and shape to that of the crystal structure whereas shrunk severely in the absence of the calcium ion as confirmed by binding–site searching results. It was also found that the calcium ion or/and conserved water molecules cause the secondary structural transitions of the active site. As a result of structural transformations, the properties of the sub–regions in the active site are greatly altered. The molecular docking results are in good agreement with the above implications from structural and property analyses.

Conclusions. The calcium ion is crucial to the maintenance of the active site of neuraminidase whereas the conserved water molecules exert a relatively small influence. The binding modes between substrates and receptors can be well predicted via structural and property analyses: sub–regions 1 and 3 (S1 and S3) are responsible for the locations of substrates whereas the orientations of substrates can be changed by sub–regions 2 and 4 (S2 and S4). Accordingly, the present results are useful to guide the substrate–receptor interaction studies and structure–based rational drug designs.

Keywords. Active site; calcium ion; conserved water molecules; neuraminidase; substrate binding.

Abbreviations and notations

NA, neuraminidase	SAS, solvent accessible surface
DANA, 2–deoxy–2, 3–dehydro–N–acetyl–neuraminic acid	CVFF, consistent valence force–field
BA, 4–(N–acetylamino)–5–guanidino–3–(3–pentyloxy) benzoic acid	EPS, electrostatic potential surface
RMSD, root–mean–square deviation	Pep, peptide fragment

* Correspondence author; phone: 0086–451–82192223; fax: 0086–451–82102082; E–mail: theobiochem@gmail.com.

1 INTRODUCTION

Influenza infection is regarded as a serious respiratory disease with significant morbidity in the general public and high mortality in elderly and high–risk patients. At present, the therapeutic measures can only provide limited control. Several molecular targets of influenza virus have been identified for the anti–influenza drugs, and among them neuraminidase (NA) receives particular attention owing to its importance [1–3]. Neuraminidase is essential for the replication of influenza virus and the infection by catalyzing the cleavage of the α–ketosidic connections between the sialic acids and the nearby sugar residues [4]. The chemical compounds that can inhibit neuraminidase will protect the hosts from viral infections. Several neuraminidase inhibitors have been approved by the Food and Drug Administration (FDA) [5–8].

With the aid of structure–based rational drug design methods, a wide variety of neuraminidase inhibitors have recently been designed [5–8]. Molecular docking is one of the most popular structure–based rational drug design methods and has established itself in the designs of neuraminidase inhibitors [9–16]. Generally, there are two ways to deal with the calcium ion and conserved water molecules present in neuraminidase: To simplify the computational models and to expedite the design processes, all the calcium ion and conserved water molecules are removed in the high–throughput molecular docking facilities [9–14]. The other option is to partially retain the calcium ion and conserved water molecules, for it has gradually been recognized that the calcium ion or/and the conserved water molecules can control the interaction strengths and rates between substrates and receptors [15–17]. The X–ray experiments [15] indicated that the absence of the calcium ion in the N9 subtype influenza virus neuraminidase causes the conformational disruptions of several loops nearby the calcium ion. The important role of the conserved water molecules was also observed during the interaction processes between substrates and neuraminidase [16], and the studies on other protein systems indicated that the conserved water molecules help to build up the hydrogen–bonded networks [18–21].

Currently, the roles of the calcium ions and the conserved water molecules in neuraminidase are far from being clearly understood. Here we obtained several different neuraminidase structures (vide post) with molecular mechanics, and the structural and property analyses were performed on these neuraminidase structures. The respective influences and roles of the calcium ion and the conserved water molecules were thus revealed. On the basis of the previous and present results, the binding modes of substrates towards the different neuraminidase structures were proposed and compared with each other. In addition, the inhibitor was docked into these neuraminidase structures to acquire the detailed interacting information and to check the implications of substrate bindings obtained from structural and property analyses. This work is useful to the substrate–receptor interaction studies and structure–based rational drug designs.

2 COMPUTATIONAL METHODOLOGY

Except where specified, all the modeling studies were performed with the modules implemented under InsightII 2005 software package (Biosym Technologies, San Diego, CA).

2.1 Preparations of Neuraminidase Structures

The three dimensional structure of N9 subtype neuraminidase was identified through the BLAST searches in the Protein Data Bank (PDB). The selected crystal structure is at 1.80 Å crystallographic resolution (PDB entry: 1F8B) [22]. All the oligosaccharides were removed from the NA structure as well as the co–complexed DANA (2–deoxy–2, 3–dehydro–N–acetyl–neuraminic acid). The protein hydrogen atoms were added at physiological pH using the Biopolymer module. As previously reported [23], the side chain of Asn294 residue in NA was rotated so that its Oδ1 and Nδ2 atoms in the amide group form hydrogen bonds instead of repulsive interactions with the nearby Ala246:O and Arg292:Nϵ2 atoms. This correction will lead to a lower root–mean–square deviation and an improved agreement with the crystal NA structure.

The roles of the calcium ion and conserved water molecules near the active site of NA were investigated with three different NA structures: (*a*) NA1, where all the calcium ion and conserved water molecules were removed; (*b*) NA2, where the calcium ion was retained whereas the conserved water molecules were removed; (*c*) NA3, where both calcium ion and conserved water molecules were retained. Note that the NA crystal structure was designated to be NA0. The previous computational results [16,24,25] indicated that two water molecules (HOH1401 and HOH3288 in the original crystal structure [22] or W1 and W2 in the present work, see their relative positions in Figure 1) are buried deep in the binding cavity and play an important role in the substrate bindings, and therefore these two water molecules are denoted as the conserved ones. Prior to the energy minimizations, each of the NA structures (NA1, NA2 and NA3) was neutralized with two chloride anions as instructed by Bonnet *et al*. [23]. Owing to the large structural distortions from the crystal state as discussed below, NA1 is extremely difficult to converge by molecular mechanics and therefore the long–time molecular dynamics (Discover 3.0 module) was executed before molecular mechanics optimizations. The conjugated gradient minimization algorithm was used to optimize the NA1, NA2 and NA3 structures (Discover 3.0 module). The consistent valence force–field (CVFF) was used and the convergence criterion was set to 0.01 kcal·mol^{-1}·Å^{-1}.

The structure of 4–(N–acetylamino)–5–guanidino–3–(3–pentyloxy) benzoic acid (abbreviated as BA) was constructed with the Builder module and shown in Figure 2. The BA substrate was optimized under B3LYP density functional theory in Gaussian 98 program [26]. The standard split–valence 6–31G(d) basis set was used, which was proven to produce reliable results in the previous work [27]. Frequency calculations at the same level were performed to confirm that the optimized structure is a minimum on potential energy surface.

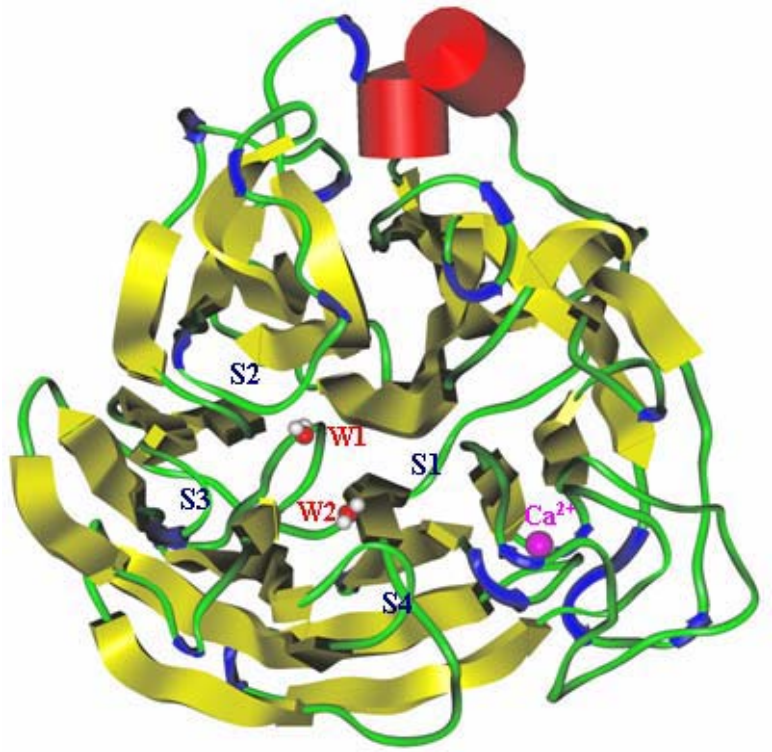

Figure 1. Ribbon diagram of N9–subtype neuraminidase structure with the calcium ion and conserved water molecules. Ribbon colors: green for random coil ribbons, blue for turns, yellow for extended strands, and red for helices. The four sub–regions in the active site were marked as S1–S4. The calcium ion (Ca^{2+}) and two conserved water molecules (W1 and W2) were drawn in ball and stick models.

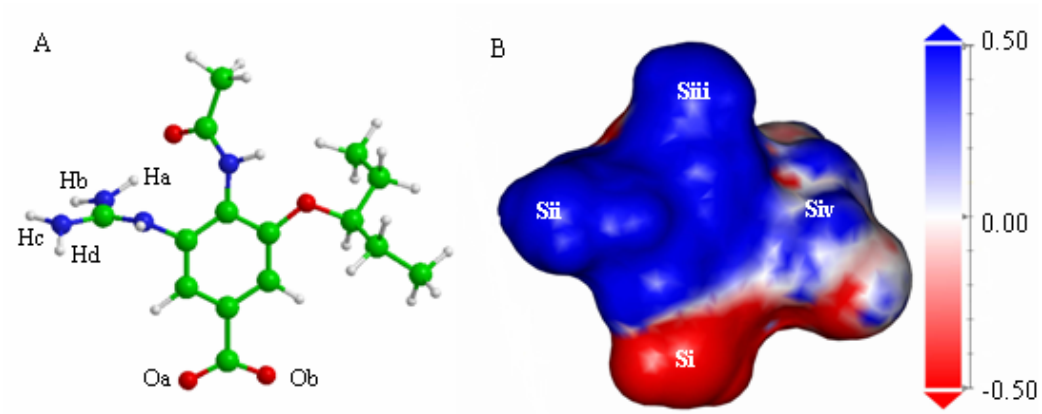

Figure 2. Chemical structure of 4–(N–acetylamino)–5–guanidino–3–(3–pentyloxy) benzoic acid (BA) as well as its electrostatic potential surface. Atom colors: C in green, N in blue O in red and H in white. The molecular surface in Figure 2B was divided into four sub–regions according to its interactions with the sub–regions of the active site in neuraminidase.

2.2 Molecular Docking

The active sites of the NA1, NA2 and NA3 structures were defined with the Binding–site module. The molecular docking simulations were performed with the advanced docking program Affinity. The consistent valence force–field (CVFF) was used and the non–bonded interactions were treated with the Cell–Multipole approach. To account for the solvent effects, the NA–BA

complexes were solvated in a sphere of TIP3P water molecules with radius of 35.0 Å which is large enough to contain the assemblies. Analogous to the above energy minimizations, two chloride anions were added to neutralize the docking systems [23]. In molecular docking simulations, the initial positions of the BA substrate were obtained using a Monte Carlo type procedure, and on the basis of energy checks 50 NA–BA structures were resulted. 40 structures of lower energies were subjected to molecular dynamics and conjugated gradient energy minimizations. The final conformations of the NA–BA complexes were obtained until the convergence criterion of the conjugated gradient minimization technique meets 0.01 kcal·mol^{-1}·Å^{-1}.

2.3 Analysis of Results

The results were analyzed with InsightII, VMD [28] and some in–house software. The NA structures under different conditions differ from each other and were characterized by the backbone–atom root–mean–square deviations (bRMSD). 14 residues were included in the active site on the basis of the previous results, with the details given in Section 3.1. The bRMSD values of the defined active site (bRMSD^{as}) were also calculated as well as the RMSD^{as} values of all the heavy atoms (aRMSD^{as}). To further characterize the structural transitions of the NA active site under different conditions, the electrostatic potential surfaces (EPS) and solvent accessible surface (SAS) areas were computed using DelPhi and Homology modules, respectively. In addition, the secondary structural elements of all the NA structures were analyzed with the ProStat module, which is based on the Kabsch–Sander method [29].

3 RESULTS AND DISCUSSION

3.1 The Active Site of Neuraminidase

Despite that 75% residue sequences are different in the NA structures of A– and B–type influenza, their active sites are well conserved [1]. In fact, the key residues of different NA structures are nearly the same, consisting of ten polar residues (Arg118, Glu119, Asp151, Arg152, Arg224, Glu227, Glu276, Glu277, Arg292 and Arg371) and four hydrophobic residues (Trp178, Ile222, Ala246, and Tyr406) [30]. Note that the N9 subtype numbering was used for the 14 key residues. As shown in Figure 1, the active site of NA3 can be divided into four sub–regions with different properties [31]. Sub–region 1 (S1) consists of a triad of arginine residues (Arg118, Arg292 and Arg371), which is positively charged and forms a hydrogen–bonded surface; Sub–region 2 (S2) contains Asp151, Glu119 and Glu227 residues and is negatively charged; Sub–region 3 (S3) is constituted by Trp178 and Ile222 residues and forms a hydrophobic cave with the nearby Arg152 residue; Sub–region 4 (S4) is a polar and hydrophobic pocket containing Glu276 and Glu277 residues. There is another hydrophobic pocket in the active site formed by the side chains of Ile222 and Ala246 residues and the hydrophobic side face of Arg224 residue [32]. However, this

hydrophobic pocket has almost no contact with substrates according to the previous experimental and calculated results and therefore will not be considered in this work [7,31,33–40].

3.2 Influences of the Calcium Ion and Conserved Water Molecules on NA Structures

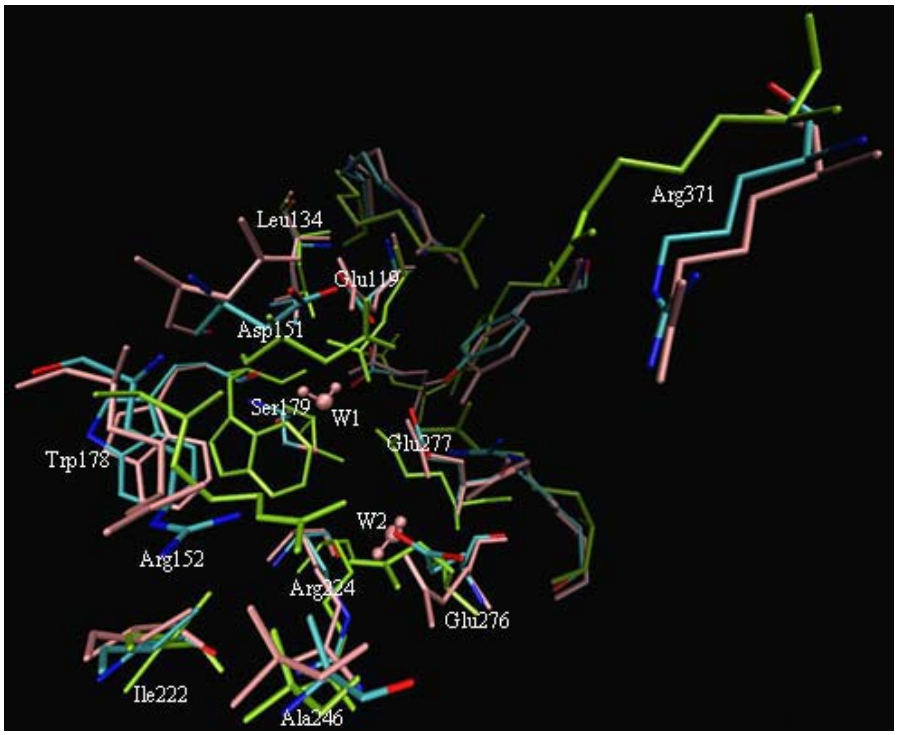

Figure 3. Stereoviews of the superposed active sites of NA1, NA2 and NA3 structures. The active sites of the NA structures were shown as stick models, and the conserved water molecules W1 and W2 in pink ball and stick models. NA2 was atom–colored (C in cyan, N in blue and O in red) whereas NA1 in olive green and NA3 in pink, respectively.

In comparison with the original crystal structure (NA0), the backbone–atom root–mean–square deviations (bRMSD) were calculated at 2.1 Å for NA1, 0.9 Å for NA2 and 1.1 Å for NA3, respectively. It indicates that the calcium ion is crucial to the maintenance of the three–dimensional structure whereas the additional two conserved water molecules exert relatively slight influences. The active sites of NA1, NA2 and NA3 structures were superposed and shown in Figure 3. It was found that the active sites of NA2 and NA3 match finely with each other. The atoms in the active site of NA1 show large position shifts relative to those in NA2 or NA3, and the Ile222:Cα–Glu276:Cα distances were used to elucidate this viewpoint. The Ile222:Cα–Glu276:Cα distances were optimized at 11.5 (0.0) Å in NA0, 10.1 (–1.4) Å in NA1, 11.3 (–0.2) Å in NA2 and 11.7 (0.2) Å in NA3, respectively. The relative distances were given in parentheses with the value of NA0 as the benchmark. The distances in NA2 and NA3 are close to each other and also approach the values in the crystal structure (NA0); however, the distances in NA1 show much larger deviations. It was interestingly found that the position shifts of the side chains of the residues are more notable than those of the backbone atoms. For example, the Ile222:CG2–Glu276:OE1 distances are equal to 9.0

(0.0) Å in NA0, 5.1 (–3.9) Å in NA1, 6.9 (–2.1) Å in NA2 and 7.0 (–2.0) Å in NA3, respectively. The Ile222 and Glu276 residues (Figure 3) belong to sub–regions 3 and 4 (S3 and S4), respectively, playing an important role in the binding properties. Therefore, the changes on the Ile222:Cα–Glu276:Cα and Ile222:CG2–Glu276:OE1 distances will result in the changes on the shapes of the active site and further on their binding properties. It should be noted here that the changes on the backbone–atom distances are generally but not always less than those of the side–chain atoms. The larger position shifts on the side chains rather than on the backbone atoms were approved by the RMSD measurements of the active site. Compared with the NA0 structure, the backbone–atom RMSD vaules of the active site ($bRMSD^{as}$) were calcualted to be 1.9 Å for NA1, 1.1 Å for NA2 and 1.2 Å for NA3, respectively. After inclusion of the heavy atoms of the side chains, the RMSD values of the active site ($aRMSD^{as}$) change to 2.7 Å for NA1, 1.4 Å for NA2 and 1.5 Å for NA3, respectively. It was found that the $aRMSD^{as}$ values in NA1, NA2 and NA3 are all larger than the corresponding $bRMSD^{as}$ values.

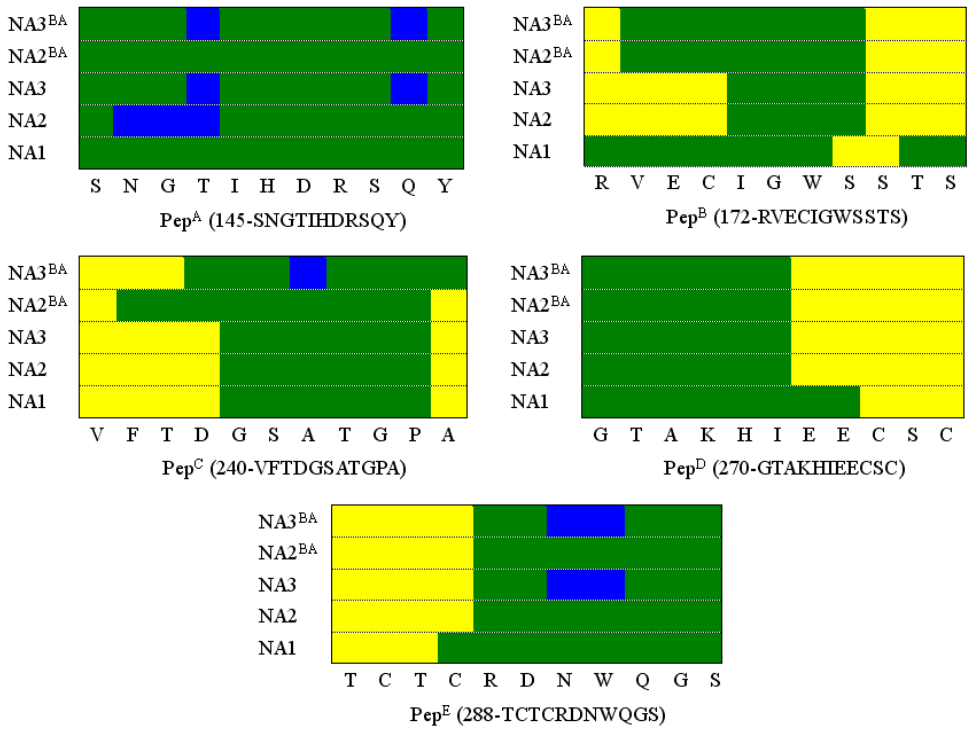

Figure 4. The secondary structural topologies of the peptide fragments in NA structures. Random coils, hydrogen–bonded turns and extended strands were shown in green, blue and yellow, respectively.

As shown in Figure 4, five representative peptide fragments were chosen to reflect the secondary structural changes of the active sites in different NA structures. The secondary structural elements of Pep^{C} (240–VFTDGSATGPA) are exactly identical in the three NA structures; however, the situations are not applicable to the other four peptide fragments. For Pep^{A} (145–SNGTIHDRSQY), Asn146, Gly147 and Tyr148 residues are of random coils in NA1 but all change to the hydrogen–bonded turns in NA2. In NA3, Asn146 and Gly147 residues are of random coils whereas the

Tyr148 residue adopts the hydrogen–bonded turn. In addition, Gln154 is characteristic of hydrogen–bonded turn in NA3, different from NA1 or NA2. It indicates that the presence of the calcium ion or/and two conserved water molecules can induce the transformations in the secondary structures of the active site. As to Pep^{E} (288–TCTCRDNWQGS), the calcium ion causes the transition of Cys291 residue from random coil (in NA1) to extended strand (in NA2), and the addition of conserved water molecules further leads to the transformations of Asn294 and Trp295 residues from random coils (in NA1 or NA2) to hydrogen–bonded turns (in NA3). As to Pep^{B} (172–RVECIGWSSTS) and Pep^{D} (270–GTAKHIEECSC), the secondary structural topologies of NA2 and NA3 are exactly the same but different from those of NA1, especially for Pep^{B} where the similarities between NA1 and NA2 (or NA3) are only present in four residues (Ile176, Gly177, Trp178 and Ser180). The transforms of the secondary structures are the natural products of the alterations of the dihedrals (Scheme 1). For instance, the dihedrals of Gly147 and Thr148 residues were optimized to be (161.1°, 69.8°) and (–149.3°, 89.5°) in NA1, (122.1°, 42.4°) and (–82.5°, 28.6°) in NA2 and (–139.4°, –71.3°) and (–62.1°, –9.8°) in NA3, respectively. The changes on the dihedrals will in turn bring about changes on the secondary structural topologies. For more data on the changes of the dihedrals, see Table 1.

Table 1. The dihedrals (°) of some selected residues in different NA structures [a]

	NA1		NA2		NA3		$NA2^{BA}$		$NA3^{BA}$	
Residue	Φ	Ψ	Φ	Ψ	Φ	Ψ	Φ	Ψ	Φ	Ψ
Asn146	–86.7	77.3	–80.5	71.0	–73.1	77.8	–86.6	68.0	–72.4	81.4
Gly147	161.1	69.8	122.1	42.4	–139.4	–71.3	112.7	89.0	–138.5	–77.3
Thr148	–149.3	89.5	–82.5	28.6	–62.1	–9.8	–143.1	130.4	–59.2	–23.0
Gln154	–76.2	–39.9	–62.1	–38.0	–67.3	–16.6	–76.9	–57.1	–62.7	–17.5
Val173	–75.2	111.4	–76.1	115.5	–73.4	117.2	–75.7	118.7	–72.5	117.5
Glu174	–93.3	–44.2	–88.7	–54.9	–77.6	–57.7	–100.6	–59.2	–76.1	–62.2
Cys175	–143.1	152.1	–150.3	163.7	–156.4	167.4	–138.8	158.7	–152.4	161.6
Ser179	–122.3	102.2	–139.5	133.1	–137.6	132.5	–135.3	155.0	–130.2	148.6
Ser180	–127.4	137.2	–145.0	152.3	–143.6	142.8	–140.2	167.4	–149.4	159.1
Thr181	–132.1	106.6	–152.0	131.1	–146.7	132.3	–164.7	134.8	–156.1	137.3
Glu276	–111.0	–94.7	–95.0	147.8	–109.5	155.9	–126.3	139.0	–131.9	137.3
Glu277	–115.5	141.0	49.3	71.2	33.4	76.5	56.9	68.7	49.7	68.8
Cys291	–92.8	148.8	–101.9	155.8	–108.5	161.3	–108.7	–177.8	–113.4	–178.9
Asn294	–87.7	58.9	–76.6	–45.5	–61.7	–47.0	–71.5	–47.0	–73.7	–50.4
Trp295	–153.5	–68.2	–57.1	–39.5	–60.5	–32.5	–53.2	–44.7	–63.4	–33.5

[a] The definition of the dihedrals for the residues can be found in Scheme 1.

3.3 Influences of the Calcium Ion and Conserved Water Molecules on NA Properties

As discussed above, the presence of the calcium ion and conserved water molecules exert remarkable influences on the sizes and shapes of the active site. Meanwhile, the secondary structures of the key residues are affected as well. The changes on the active site structures will bring about the changes in their properties such as hydrogen bonds, electrostatic potential surfaces (EPS), and solvent accessible surfaces (SAS) areas.

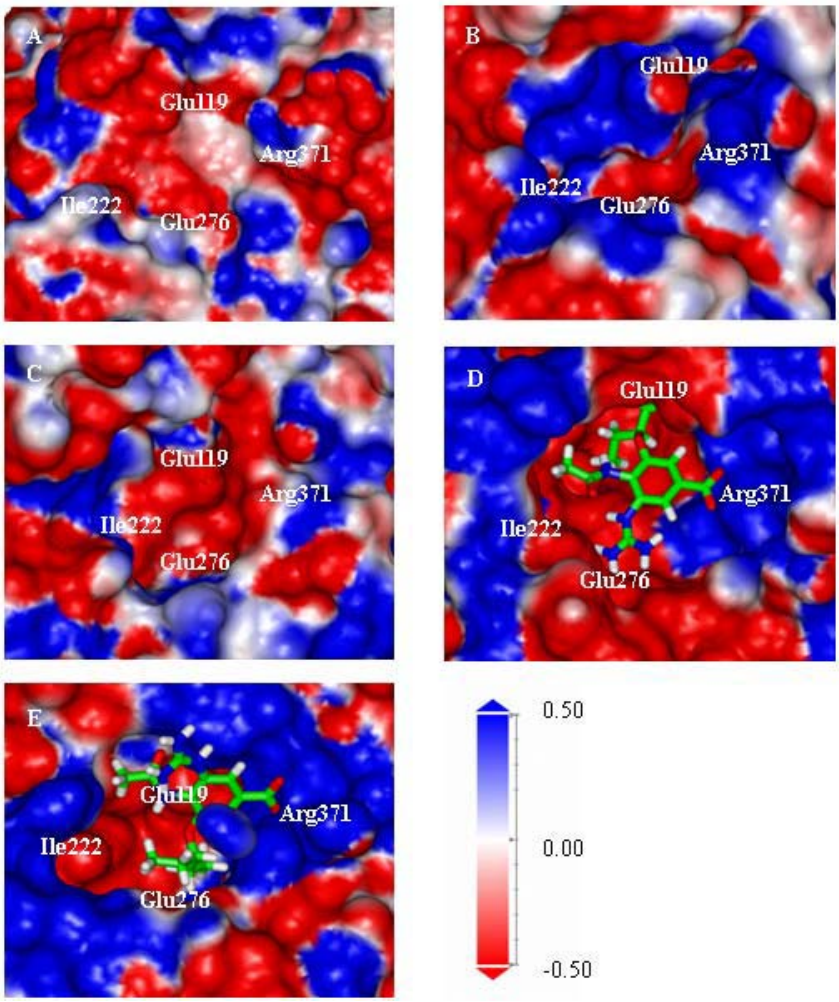

Figure 5. Electrostatic potential surfaces of the active sites of A. NA1, B. NA2, C. NA3, D. $NA2^{BA}$ and E. $NA3^{BA}$, respectively. The active sites were defined through Binding Site Analysis module. The NA structures were colored by electrostatic potentials. The BA substrate was shown in stick model.

Table 2. Hydrogen bonds between the crystal water molecules and residues in NA3

Water molecule	Residue	Atom	Distance (Å)	Angle (°)
W1	Trp178:O	HO1	2.16	152.98
	Ser179:OH	O	1.88	157.52
	Glu227:OE1	HO2	1.93	157.41
W2	Arg224:NE	HO1	2.33	170.37
	Glu277:HN	O	2.19	161.46
	Glu277:OE1	HO2	2.14	147.08

The electrostatic potential surfaces (EPS) of the active sites in NA1, NA2 and NA3 were shown in Figure 5. Compared with NA2, the positive charged sub–region 1 (S1) in NA1 is greatly reduced and covered up by the residues near the active site; the positive charged sub–region 4 (S4) is also reduced somewhat and meanwhile extruded towards the active site. The calcium ion in NA2 shows electrostatic attractions towards the negative charged Glu276 and Glu277 residues. Through the electrostatic interactions, the calcium ion can further modulate the shape of the active site, which is in agreement with the position–shift and RMSD results discussed above. In NA1, two salt bridges

were formed between the carboxylic group of Asp151 residue and the guanidinium groups of Arg118 and Arg292 residues, which are however absent in NA2. As a result of the formed salt bridges, the Asp151 residue in NA1 was tightly trapped and its affinity towards substrates was substantially depressed. To summarize, the active site of NA1 shrinks greatly as a result of the movements of the residues, which may cause the disruptions to the catalytic properties. It is consistent with the experimental results that the active site of neuraminidase is stabilized by the calcium ion that is necessary for the bioactivities [15,41].

In contrast to the positive–charge dominated active site in NA2 (Figure 5B), more negative charged regions are present in the NA3 active site as displayed in the EPS of Figure 5C, and the charge redistribution was caused by the addition of two conserved water molecules (W1 and W2). W1 and W2 in NA3 show electrostatic interactions towards the residues in the active site and result in the reduction of the positive charges in sub–regions 1, 2 and 4 (S1, S2 and S4). In addition, these two water molecules (W1 and W2) form three hydrogen bonds with Trp178, Ser179, Glu227 and Arg224, Glu277, Glu277 residues, respectively, with their geometric details listed in Table 2. As a result, these residues move towards the W1 and W2 molecules and in turn cause the position shifts of the adjacent residues.

Table 3. The solvent accessible surface areas (Å^2) of the active site residues in different NA structures. Calculated for polar areas (P) and non–polar areas (N)

	NA1		NA2		NA3	
Monomer	P	N	P	N	P	N
Arg118	0.00	4.51	26.42	5.56	30.08	1.23
Glu119	0.47	0.00	3.27	4.24	7.62	0.00
Asp151	0.00	0.00	35.04	21.85	14.55	28.18
Arg152	20.52	11.65	90.56	16.35	101.84	13.23
Trp178	0.00	0.00	6.68	5.71	0.00	4.63
Ile222	0.00	21.18	0.00	20.20	0.00	12.34
Arg224	0.00	0.00	1.17	3.86	1.17	6.95
Glu227	0.00	0.00	0.93	0.00	0.00	0.00
Ala246	1.21	5.09	0.39	5.94	5.16	14.58
Glu276	0.00	0.00	4.67	0.19	2.33	1.93
Glu277	0.00	0.00	12.68	4.57	14.85	1.34
Arg292	0.00	0.00	39.86	0.00	33.16	0.27
Arg371	26.88	0.00	35.28	24.16	33.49	14.09
Tyr406	0.39	0.00	2.57	5.51	6.54	9.99
Sum	49.47	42.43	259.52	118.14	250.79	108.76

The solvent accessible surface (SAS) areas of the residues in the active site, including the polar and nonpolar SAS areas, were calculated and some of the values were listed in Table 3. The polar and nonpolar areas of the residues in the active site were summed to 49.47 and 42.43 Å^2 in NA1, 259.52 and 118.14 Å^2 in NA2 and 250.79 and 108.76 Å^2 in NA3, respectively. The polar and nonpolar as well as the total SAS areas are greatly reduced in the case of NA1, where neither the calcium ion nor the conserved water molecules are present. Albeit the total values of NA2 and NA3 are close to each other, the values of the individual residues may have noticeable differences. In

consistency with the great reductions in the total polar, nonploar and SAS areas, the values of the individual residues in NA1 are very low, and for Asp151, Trp178, Arg224, Glu227, Glu276, Glu277 and Arg292 residues the polar, nonploar and SAS areas are all reduced to nearly zero. It indicates that the absence of the calcium ion will cause the collapse of the active site, in agreement with the RMSD and EPS results. Compared with NA2, the polar and nonpolar areas of Asp151 residue in NA3 change from 35.04 and 21.85 $Å^2$ to 14.55 and 28.18 $Å^2$, respectively, suggesting that sub–region 2 (S2) shows more polar in NA2 whereas more nonpolar in NA3. For sub–region 4 (S4), the polar and nonpolar areas of Glu276 residue change from 4.67 to 2.33 $Å^2$ and from 0.19 to 1.93 $Å^2$, respectively; the polar and nonpolar areas of Glu277 residue change from 12.68 to 14.85 $Å^2$ and 4.57 to 1.34 $Å^2$, respectively. It indicates that Glu276 residue in NA2 and Glu277 residue in NA3 show predominately polar while the proportions of polar areas are decreased in Glu277 residue in NA2 and Glu276 residue in NA3 as a result of the increased proportions of nonpolar areas. It indicates the two conserved water molecules can tune the hydrophilic and hydrophobic properties of the individual residues and further of the sub–regions in the active site. Accordingly, the binding modes and strengths of the substrates will be affected by the presence of the calcium ion or/and conserved water molecules.

3.4 Binding Properties of BA with Different NA Structures

As shown in the binding–site module, there is no vacant space enough in the active site of NA1 to hold the BA substrate. That is, the BA substrate can not be docked into the NA structure in the absence of the calcium ion. NA2 and NA3 were found to have enough spaces to hold the BA substrate. The combined complexes $NA2^{BA}$ and $NA3^{BA}$ were obtained and optimized as described in Section 2.2. It can be clearly seen from Figure 6 that the locations of BA are different in $NA2^{BA}$ and $NA3^{BA}$ and as a result the interacted residues in the active site show differences as well. The total interaction energies were calculated to be –217.78 kcal·mol^{-1} in $NA2^{BA}$ and –117.76 kcal·mol^{-1} in $NA3^{BA}$, respectively. The electrostatic interactions rather than van der Waals play more noticeable roles in both cases, with their values (proportions) equaling –178.34 kcal·mol^{-1} (81.9%) in $NA2^{BA}$ and –90.91 kcal·mol^{-1} (77.2%) in $NA3^{BA}$, respectively. The strong electrostatic attractions can also be observed from the electrostatic potential maps drawn in Figures 5D and 5E, consistent with the experimental and docking results of the other inhibitors such as zanamivir and oseltamivir [14,23,32,42]. Apart from the differences in the locations, the interacting directions of BA differ when combined with NA2 and NA3. In $NA2^{BA}$, the guanidinium group of BA is combined with sub–region 4 (S4) through electrostatic interactions with Glu276 and Glu277 residues; however, this guanidinium group was pushed aside and faces opposite to the active site in $NA3^{BA}$. The hydrogen bonds between BA and NA structures were listed in Table 4. Six and three hydrogen bonds were formed in $NA2^{BA}$ and $NA3^{BA}$, respectively; moreover, none of the formed hydrogen bonds are identical in $NA2^{BA}$ and $NA3^{BA}$. The carboxyl group in BA was found to be a

pivotal site and forms four and three hydrogen bonds with the active sites of NA2 and NA3, respectively.

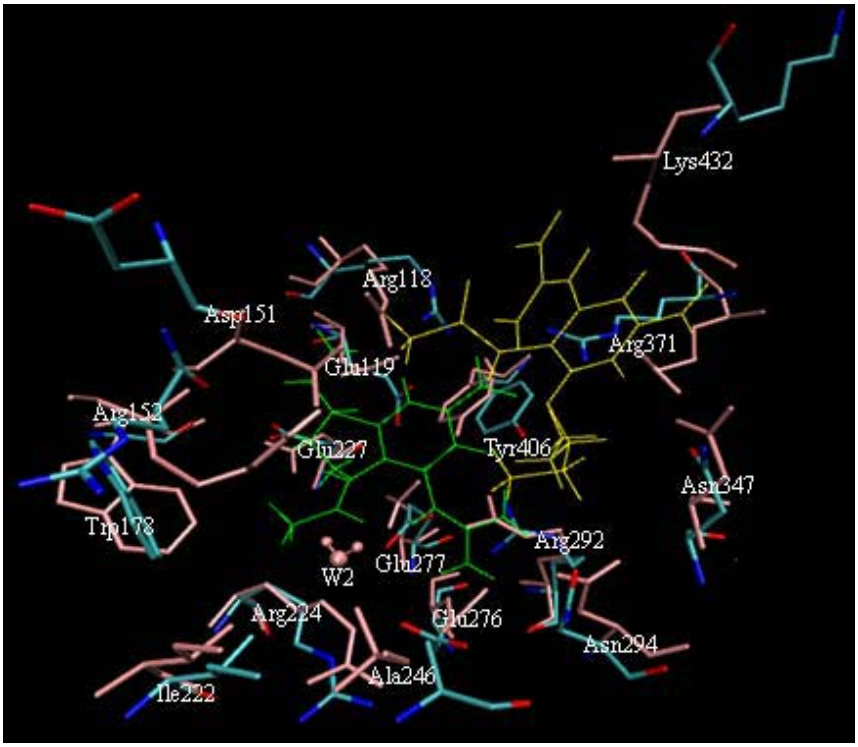

Figure 6. Stereoviews of the superposed active sites of $NA2^{BA}$ and $NA3^{BA}$ structures docked with the BA substrates. The active sites of NA structures were shown as stick models, with NA2 atom–colored (C in cyan, N in blue and O in red) and NA3 in pink, respectively. The conserved water molecules are in pink and in ball and stick models. The BA substrates in $NA2^{BA}$ and $NA3^{BA}$ were displayed in green and yellow line models, respectively.

Table 4. Hydrogen bonds between BA and residues in the active sites of different NA structures

	Residue	Ligand	Distance (Å)	Angle (°)
$NA2^{BA}$	Arg118:NH21	Ob	1.78	147.40
	Glu276:OE2	Ha	2.31	147.91
	Asn294:OD2	Hb	2.08	160.57
	Arg371:NH11	Oa	1.65	161.40
	Arg371:NH21	Ob	1.86	171.68
	Tyr406:OH	Oa	1.59	170.59
$NA3^{BA}$	Asn347:HD22	Ob	1.98	166.70
	Arg371:NH11	Ob	1.95	141.65
	Lys432:HZ3	Ob	1.90	178.11

From the electrostatic surface maps in Figure 5D and 5E, it can be found that BA is well contained in the active site of $NA2^{BA}$ whereas some parts protrude outside the active site of $NA3^{BA}$. In $NA3^{BA}$, W1 is expelled away from the original position as a result of the attacks of the guanidinium and N–acetyl groups of BA towards sub–regions 2 and 3 (S2 and S3) W1 in NA3 obstructs the attacks and therefore the interactions between BA and S2, S3 are somewhat weaken in $NA3^{BA}$ compared with $NA2^{BA}$. The displacement of W2 due to the docking of BA is slight. W2 stabilizes the polar sub–region 4 (S4) but meanwhile blocks the entrance of BA to S4. Accordingly,

the interacting modes and strengths between BA and NA structures (NA2 and NA3) have remarkable differences owing to the presence of two conserved water molecules in NA3. It was thus shown that the conserved water molecules are important in the substrate bindings, and with the inclusion of conserved water molecules the docking simulations produce satisfactory agreements with the experimental results [16,23,24,42,43].

3.5 Implications from Structural and Property Analyses: Comparisons with Docking Results

From the structural and property analyses on different NA structures (NA1, NA2 and NA3), some important clues on substrate bindings can be predicted. BA was optimized with B3LYP/6–31G(d) methods, and frequency calculations at the same level of theory were performed confirming that this structure is an energy minimum. According to the division strategy of the NA3 active site (Figure 1), BA was divided into four sub–regions and shown in Figure 2: sub–region i (Si) is a carboxylated anion (COO^-), sub–region ii (Sii) contains a guanidinium group ($[NH=C(NH_2)_2]^+$), sub–region iii (Siii) is a N–acetyl group and displays mainly positive charge; sub–region iv (Siv) is a neutral O–butane group of hydrophobic nature.

As described in Sections 3.2 and 3.3, the active site of NA1 shrinks remarkably so that the BA substrate can not be located into its "pocket" (Figure 5A), consistent with the binding–site–searching result using Binding–site module. The structural analyses showed that there are "pockets" in NA2 and NA3 (Figures 5B and 5C) but the properties of their active sites are different, in good agreement with the binding–site–searching and docking results (Figures 5D and 5E). The total SAS areas of the active sites were calculated to be 377.66 $Å^2$ for NA2 and 359.55 $Å^2$ for NA3, respectively. Accordingly, the active sites of NA2 and NA3 are large enough to hold BA whose SAS area equals 345.29 $Å^2$. Moreover, the proteins are flexible in structure and can dock substrates with larger sizes than forecasted from the SAS areas [44]. As a result of the mutual interactions between BA and NA structures, the active sites were expanded with the SAS areas equaling 544.27 $Å^2$ for NA2 and 385.92 $Å^2$ for NA3, respectively. The structures and properties of the active site of NA2 and NA3 have evident discrepancies, and accordingly there are displacements in the residues and sub–regions between these two NA structures as superposed in Figure 6. It was found that sub–regions 1 and 3 (S1 and S3) determine the locations of substrates (Figure 6): the two positive–charged guanidinium groups of Arg292 and Arg371 residues in S1 will bind through electrostatic interactions and hydrogen bonds with the negative–charged carboxylated group of BA; i.e., sub–region i (Si) in Figure 2. Meanwhile, the hydrophobic Trp178 and Ile222 residues in S3 match the N–acetyl group of BA; i.e., sub–region iii (Siii). Sub–regions 2 and 4 (S2 and S4) contribute to the further stabilizations of the formed complexes. As described in Section 3.1, S2 and S4 show negative charges and hydrophobic properties and therefore these two sub–regions in NA3 will bind the guanidinium group and O–butyl group of BA; *i.e.*, sub–region ii (Sii) and sub–region iv (Siv) in

Figure 2, respectively. However, both W1 (vicinal to S2) and W2 (vicinal to S4) are absent in NA2, causing the increases of polarity in S2 and negative charges in S4. As a result, in $NA2^{BA}$ the guanidinium group (Sii) and the O–butyl group (Siv) of BA are bound with S4 and S2, respectively. That is, the orientations of BA in $NA2^{BA}$ and $NA3^{BA}$ are different owing to the structural and property differences in NA2 and NA3. Accordingly, the interaction modes between substrates and receptors can be predicted from the structural and property analyses.

4 CONCLUSIONS

In this work, three different neuraminidase structures (NA1 in the absence of the calcium ion and conserved water molecules, NA2 in the presence of the calcium ion and NA3 in the presence of both calcium ion and conserved water molecules) were optimized and analyzed, revealing the roles of the calcium ion or/and conserved water molecules in substrate bindings with neuraminidase. In addition, density functional theory and molecular docking methods were employed to study the mutual interactions between substrates and NA structures, and the docking results were compared with those implicated from structural and property analyses. The present results are useful to guide the substrate–receptor studies and structure–based rational drug designs.

As indicated by the root–mean–square deviations (RMSD) and the position shifts of key residues, the shapes and sizes of the active sites of NA2 and NA3 are close to those in the original crystal structure whereas not so in the case of NA1. The calcium ion is crucial to the maintenance of the active site while the additional two conserved water molecules exert relatively slight influences. Moreover, larger structural movements were observed in the side chains of the key residues rather than in their backbone atoms. Either the calcium ion or the conserved water molecules can cause the secondary structural transitions of the five key peptide fragments at the active site.

As a result of structural transformations, the properties of the four sub–regions in the active site are greatly altered by the presence of the calcium ion (NA2 vs. NA1), with the details of electrostatic potential surfaces (EPS) and solvent accessible surfaces (SAS) areas provided in the discussions. It was also found that the active site in NA1 shrinks remarkably so that substrates can not be located into its “pocket”, consistent with the binding–site–searching results. Although the structural differences between NA2 and NA3 are relatively slight, the charges, hydrophilicity vs. hydrophobicity and polarity vs. nonpolarity were redistributed in the sub–regions of these two structures. The structural and property analyses implicated that sub–regions 1 and 3 (S1 and S3) are responsible for the locations of substrates in the active site whereas the orientations of the substrates can be tuned by sub–regions 2 and 4 (S2 and S4).

The docking results (Figure 6) are in excellent agreement with the structural and property implications, indicating that the interaction modes between substrates and receptors are determined

by their structures and properties and can therefore be predicted. The docking results showed that the total interaction energies with BA were calculated to be –217.78 kcal·mol^{-1} for NA2 and –117.76 kcal·mol^{-1} for NA3, respectively. In addition, the electrostatic interactions rather than van der Waals were found to play a more important role.

Acknowledgment

The Talented Funds of Northeast Forestry University (No. 220–602042) and the Chinese Postdoc Foundation (No. 20060400802) were acknowledged.

5 REFERENCES

[1] E. Garman and G. Laver. Controlling Influenza by Inhibiting the Virus's Neuraminidase. *Curr. Drug Targets*. **2004**, *5*, 119–136.
[2] A. Moscona. Neuraminidase Inhibitors for Influenza. *New. Engl. J. Med*. **2005**, *353*, 1363–1373.
[3] J. R. Rupert, F. H. Lesley, J. S. David, J. C. Patrick, P.–L. Yi, B. G. Michael, J. H. Alan, J. G. Steven, and J. S. John. The Structure of H5N1 Avian Influenza Neuraminidase Suggests New Opportunities for Drug Design. *Nature* **2006**, *443*, 45–49.
[4] P. Sears and C. H. Wong. Carbohydrate Mimetics: A New Strategy for Tackling the Problem of Carbohydrate–Mediated Biological Recognition. *Angew. Chem. Int. Ed*. **1999**, *38*, 2300–2324.
[5] N. R. Taylor, A. Cleasby, O. Singh, T. Skarzynski, A. J. Wonacott, P. W. Smith, S. L. Sollis, P. D. Howes, P. C. Cherry, R. Bethell, P. Colman, and J. Varghese. Dihydropyrancarboxamides Related to Zanamivir: a New Series of Inhibitors of Influenza Virus Sialidases. 2. Crystallographic and Molecular Modeling Study of Complexes of 4–amino–4H–pyran–6–carboxamides and Sialidase from Influenza Virus Types A and B. *J. Med. Chem*. **1998**, *41*, 798–807.
[6] J. N. Varghese, P. W. Smith, S. L. Sollis, T. J. Blick, A. Sahasrabudhe, J. L. Mc–Kimm–Breschin, and P. M. Colman. Drug Design Against a Shifting Target: a Structural Basis for Resistance to Inhibitors in a Variant of Influenza Virus Neuraminidase. *Structure* **1998**, *6*, 735–746.
[7] Y. S. Babu, P. Chand, S. Bantia, P. Kotian, A. Dehghani, Y. El–Kattan, T. H. Lin, T. L. Hutchison, A. J. Elliott, C. D. Parker, S. L. Ananth, L. L. Horn, G. W. Laver, and J. A. Montgomery. BCX–1812 (RWJ–270201): Discovery of a Novel, Highly Potent, Orally Active, and Selective Influenza Neuraminidase Inhibitor Through Structure–based Drug Design. *J. Med. Chem*. **2000**, *43*, 3482–3486.
[8] B. J. Smith, J. L. McKimm–Breshkin, M. McDonald, R. T. Fernley, J. N. Varghese, and P. M. Colman. Structural Studies of the Resistance of Influenza Virus Neuramindase to Inhibitors. *J. Med. Chem*. **2002**, *45*, 2207–2212.
[9] C. W. Murray, C. A. Baxter and A. D. Frenkel. The Sensitivity of the Results of Molecular Docking to Induced Fit Effects: Application to Thrombin, Thermolysin and Neuraminidase. *J. Comput. Aided Mol. Des*. **1999**, *13*, 547–562.
[10] X. Yi, Z. Guo, and F. M. Chu. Study on Molecular Mechanism and 3D–QSAR of Influenza Neuraminidase Inhibitors. *Bioorg. Med. Chem*. **2003**, *11*, 1465–1474.
[11] M. C. Mann, T. Islam, J. C. Dyason, P. Florio, C. J. Trower, R. J. Thomson, and M. von Itzstein. Unsaturated N–acetyl–D–glucosaminuronic Acid Glycosides as Inhibitors of Influenza Virus Sialidase. *Glycoconj J*. **2006**, *23*, 127–133.
[12] D. Platis, B. J. Smith, T. Huyton, and N. E. Labrou. Structure–guided Design of a Novel Class of Benzyl–sulfonate Inhibitors for Influenza Virus Neuraminidase. *Biochem J*. **2006**, *399*, 215–223.
[13] C. Sun, X. Zhang, H. Huang, and P. Zhou. Synthesis and Evaluation of a New Deries of Substituted Acyl(thio)urea and Thiadiazolo [2,3–α] Pyrimidine Derivatives as Potent Inhibitors of Influenza Virus Neuraminidase. *Bioorg Med Chem*. **2006**, *14*, 8574–8581.
[14] M. Zheng, K. Yu, H. Liu, X. Luo, K. Chen, W. Zhu, and H. Jiang. QSAR Analyses on Avian Influenza Virus Neuraminidase Inhibitors Using CoMFA, CoMSIA, and HQSAR. *J Comput Aided Mol Des*. **2006**, *20*, 549–566.
[15] B. J. Smith, T. Huyton, R. P. Joosten, J. L. McKimm–Breschkin, J. G. Zhang, C. S. Luo, M. Z. Lou, N. E. Labrou, and T. P. J. Garrett. Structure of a Calcium–deficient Form of Influenza Virus Neuraminidase: Implications for Substrate Binding. *Acta. Crystallogr. D*. **2006**, *62*, 947–952.
[16] C. Barillari, J. Taylor, R. Viner, and J. W. Essex. Classification of Water Molecules in Protein Binding Sites. *J. Am. Chem. Soc*. **2007**, *129*, 2577–2587.

[17] A. K. Chong, M. S. Pegg, and M. von Itzstein. Influenza Virus Sialidase: Effect of Calcium on Steady–state Kinetic Parameters. *Biochim*. *Biophys*. *Acta* **1991**, *1077*, 65–71.
[18] J. D. Dunitz. The Entropic Cost of Bound Water in Crystals and Biomolecules. *Science* 1994, 264, 670.
[19] C. de Graaf, P. Pospisil, W. Pos, G. Folkers, and N. P. E. Vermeulen. Binding Mode Prediction of Cytochrome P450 and Thymidine Kinase Protein–ligand Complexes by Consideration of Water and Rescoring in Automated Docking. *J*. *Med*. *Chem*. **2005**, *48*, 2308–2318.
[20] M. L. Verdonk, G. Chessari, J. C. Cole, M. J. Hartshorn, C. W. Murray, J. W. M. Nissink, R. D. Taylor, and R. Taylor. Modeling Water Molecules in Protein–ligand Docking Using GOLD. *J*. *Med*. *Chem*. **2005**, *48*, 6504–6515.
[21] A. T. Garcia–Sosa and R. L. Mancera. The Effect of a Tightly Bound Water Molecule on Scaffold Diversity in the Computer–aided de Novo Ligand Design of CDK2 Inhibitors. *J*. *Mol*. *Model*. **2006**, *12*, 422–431.
[22] B. J. Smith, P. M. Colman, M. Von Itzstein, B. Danylec, and J. N. Varghese. Analysis of Inhibitor Binding in Influenza Virus Neuraminidase. *Protein Sci*. **2001**, *10*, 689–696.
[23] P. Bonnet and R. A. Bryce. Molecular Dynamics and Free Energy Analysis of Neuraminidase–ligand Interactions. *Protein Sci*. **2004**, *13*, 946–957.
[24] R. L. Mancera. De Novo Ligand Design with Explicit Water Molecules: an Application to Bacterial Neuraminidase. *J*. *Comput*. *Aided Mol*. *Des*. **2002**, *16*, 479–499.
[25] L. Birch, C. W. Murray, M. J. Hartshorn, I. J. Tickle, and M. L. Verdonk. Sensitivity of Molecular Docking to Induced Fit Effects in Influenza Virus Neuraminidase. *J*. *Comput*. *Aided Mol*. *Des*. **2002**, *16*, 855–869.
[26] M. J. Frisch, G. W. Trucks, H. B. Schlegel, G. E. Scuseria, M. A. Robb, J. R. Cheeseman, V. G. Zakrzewski, J. A. Montgomery Jr., R. E. Stratmann, J. C. Burant, S. Dapprich, J. M. Millam, A. D. Daniels, K. N. Kudin, M. C. Strain, O. Farkas, J. Tomasi, V. Barone, M. Cossi, R. Cammi, B. Mennucci, C. Pomelli, C. Adamo, S. Clifford, J. Ochterski, G. A. Petersson, P. Y. Ayala, Q. Cui, K. Morokuma, D. K. Malick, A. D. Rabuck, K. Raghavachari, J. B. Foresman, J. Cioslowski, J. V. Ortiz, A. G. Baboul, B. B. Stefanov, G. Liu, A. Liashenko, P. Piskorz, I. Komaromi, R. Gomperts, R. L. Martin, D. J. Fox, T. Keith, M. A. Al–Laham, C. Y. Peng, A. Nanayakkara, C. Gonzalez, M. Challacombe, P. M. W. Gill, B. Johnson, W. Chen, M. W. Wong, J. L. Andres, C. Gonzalez, M. Head–Gordon, E. S. Replogle, and J. A. Pople. Gaussian 98, Revision A.9, Gaussian, Inc., Pittsburgh, PA, (1998).
[27] G. Yang, X. W. Han, X. M. Liu, P. Y. Yang, Y. G. Zhou, and X. H. Bao. Study on Conformation Interconversion of 3–alkyl–4–acetyl–3,4–dihydro–2H– 1,4– benzo– xazines from Dynamic NMR Experiments and Ab Initio Density Functional Calculations. *J*. *Phys*. *Chem*. *B* **2005**, *109*, 18690–18698.
[28] W. Humphrey, A. Dalke, and K. Schulten. VMD: Visual Molecular Dynamics. *J*. *Mol*. *Graph*. **1996**, *14*, 33–38.
[29] W. Kabsch and C. Sander. Dictionary of Protein Secondary Structure: Pattern Recognition of Hydrogen–bonded and Geometrical Features. *Biopolymers* **1983**, *22*, 2577–2637.
[30] R. C. Wade. 'Flu' and Structure–based Drug Design. *Structure* **1997**, *5*, 1139–1145.
[31] G. T. Wang, Y. W. Chen, S. Wang, R. Gentles, T. Sowin, W. Kati, S. Muchmore, V. Giranda, K. Stewart, H. Sham, D. Kempf, and W. G. Laver. Design, Synthesis, and Structural Analysis of Influenza Neuraminidase Inhibitors Containing Pyrrolidine Cores. *J*. *Med*. *Chem*. **2001**, *44*, 1192–1201.
[32] V. Stoll, K. D. Stewart, C. J. Maring, S. Muchmore, V. Giranda, Y. G. Gu, G. Wang, Y. W. Chen, M. H. Sun, C. Zhao, A. L. Kennedy, D. L. Madigan, Y. B. Xu, A. Saldivar, W. Kati, G. Laver, T. Sowin, H. L. Sham, J. Greer, and D. Kempf. Influenza Neuraminidase Inhibitors: Structure–based Design of a Novel Inhibitor Series. *Biochemistry* **2003**, *42*, 718–727.
[33] P. Chand, Y. S. Babu, S. Bantia, N. Chu, L. B. Cole, P. L. Kotian, W. G. Laver, J. A. Montgomery, V. P. Pathak, S. L. Petty, D. P. Shrout, D. A. Walsh, and G. M. Walsh. Design and Synthesis of Benzoic Acid Derivatives as Influenza Neuraminidase Inhibitors Using Structure–based Drug Design. *J*. *Med*. *Chem*. **1997**, *40*, 4030–4052.
[34] M. A. Williams, W. Lew, D. B. Mendel, C. Y. Tai, P. A. Escarpe, W. G. Laver, R. C. Stevens, and C. U. Kim. Structure–activity Relationships of Carbocyclic Influenza Neuraminidase Inhibitors. *Bioorg*. *Med*. *Chem*. *Lett*. **1997**, *7*, 1837–1842.
[35] C. U. Kim, W. Lew, M. A. Williams, H. W. Wu, L. J. Zhang, X. W. Chen, P. A. Escarpe, D. B. Mendel, W. G. Laver, and R. C. Stevens. Structure–activity Relationship Studies of Novel Carbocyclic Influenza Neuraminidase Inhibitors. *J*. *Med*. *Chem*. **1998**, *41*, 2451–2460.
[36] W. Lew, H. W. Wu, D. B. Mendel, P. A. Escarpe, X. W. Chen, W. G. Laver, B. J. Graves, and C. U. Kim. A new Series of C_3–aza Carbocyclic Influenza Neuraminidase Inhibitors: Synthesis and Inhibitory Activity. *Bioorg*. *Med*. *Chem*. *Lett*. **1998**, *8*, 3321–3324.
[37] V. R. Atigadda, W. J. Brouillette, F. Duarte, S. M. Ali, Y. S. Babu, S. Bantia, P. Chand, N. M. Chu, J. A. Montgomery, D. A. Walsh, E. A. Sudbeck, J. Finley, M. Luo, G. M. Air, and G. W. Laver. Potent Inhibition of Influenza Sialidase by a Benzoic Acid Containing a 2–Pyrrolidinone Substituent. *J*. *Med*. *Chem*. **1999**, *42*, 2332–2343.
[38] P. Chand, Y. S. Babu, S. Bantia, S. Rowland, A. Dehghani, P. L. Kotian, T. L. Hutchison, S. Ali, W. Brouillette, Y. El–Kattan, and T. H. Lin. Syntheses and Neuraminidase Inhibitory Activity of Multisubstituted Cyclopentane

Amide Derivatives. *J. Med. Chem*. **2004**, *47*, 1919–1929.
[39] C. J. Maring, V. S. Stoll, C. Zhao, M. H. Sun, A. C. Krueger, K. D. Stewart, D. L. Madigan, W. M. Kati, Y. B. Xu, R. J. Carrick, D. A. Montgomery, A. Kempf–Grote, K. C. Marsh, A. Molla, K. R. Steffy, H. L. Sham, W. G. Laver, Y. G. Gu, D. J. Kempf, and W. E. Kohlbrenner. Structure–based Characterization and Optimization of Novel Hydrophobic Binding Interactions in a Series of Pyrrolidine Influenza Neuraminidase Inhibitors. *J. Med. Chem*. **2005**, *48*, 3980–3990.
[40] G. Yang, Z. W. Yang, X. M. Wu, and Y. G. Zu. A Novel Anti–influenza Drug: Molecular Docking of Trihydroxymethoxyflavone. *Chin. Comput. Appl. Chem*. **2008**, *25*, 409–414.
[41] T. Takahashi, T. Suzuki, K. I. Hidari, D. Miyamoto, and Y. Suzuki. A Molecular Mechanism for the Low–pH Stability of Sialidase Activity of Influenza A Virus N2 Neuraminidases. *FEBS. Lett*. **2003**, *543*, 71–75.
[42] K. M. Masukawa, P. A. Kollman, and I. D. Kuntz. Investigation of Neuraminidase–substrate Recognition Using Molecular Dynamics and Free Energy Calculations. *J. Med. Chem*. **2003**, *46*, 5628–5637.
[43] V. R. Atigadda, W. J. Brouillette, F. Duarte, Y. S. Babu, S. Bantia, P. Chand, N. M. Chu, J. A. Montgomery, D. A. Walsh, E. Sudbeck, J. Finley, G. M. Air, M. Luo, and G. W. Laver. Hydrophobic Benzoic Acids as Inhibitors of Influenza Neuraminidase. *Bioorg. Med. Chem*. **1999**, *7*, 2487–2497.
[44] N. Brooijmans and I. D. Kuntz. Molecular Recognition and Docking Algorithms. *Annu. Rev. Biophys. Biomol. Struct*. **2003**, *32*, 335–373.